Developmental Cell
Article

The Vps27/Hse1 Complex Is a GAT Domain-Based Scaffold for Ubiquitin-Dependent Sorting

Gali Prag,[1] Hadiya Watson,[2] Young C. Kim,[3] Bridgette M. Beach,[1] Rodolfo Ghirlando,[1] Gerhard Hummer,[3] Juan S. Bonifacino,[2] and James H. Hurley[1,*]
[1] Laboratory of Molecular Biology, National Institute of Diabetes and Digestive and Kidney Diseases
[2] Cell Biology and Metabolism Branch, National Institute of Child Health and Human Development
[3] Laboratory of Chemical Physics, National Institute of Diabetes and Digestive and Kidney Diseases
National Institutes of Health, U.S. Department of Health and Human Services, Bethesda, MD 20892, USA
*Correspondence: jh8e@nih.gov
DOI 10.1016/j.devcel.2007.04.013

SUMMARY

The yeast Vps27/Hse1 complex and the homologous mammalian Hrs/STAM complex deliver ubiquitinated transmembrane proteins to the ESCRT endosomal-sorting pathway. The Vps27/Hse1 complex directly binds to ubiquitinated transmembrane proteins and recruits both ubiquitin ligases and deubiquitinating enzymes. We have solved the crystal structure of the core responsible for the assembly of the Vps27/Hse1 complex at 3.0 Å resolution. The structure consists of two intertwined GAT domains, each consisting of two helices from one subunit and one from the other. The two GAT domains are connected by an antiparallel coiled coil, forming a 90 Å-long barbell-like structure. This structure places the domains of Vps27 and Hse1 that recruit ubiquitinated cargo and deubiquitinating enzymes close to each other. Coarse-grained Monte Carlo simulations of the Vps27/Hse1 complex on a membrane show how the complex binds cooperatively to lipids and ubiquitinated membrane proteins and acts as a scaffold for ubiquitination reactions.

INTRODUCTION

Protein ubiquitination is a widespread, multifunctional regulatory mechanism. Ubiquitin is conjugated to proteins via an isopeptide bond between the C terminus of ubiquitin and Lys residues in the ubiquitinated protein. This reaction is carried out by a ubiquitin-activating enzyme (E1), a ubiquitin-conjugating enzyme (E2), and a ubiquitin protein ligase (E3) (Hershko et al., 2000; Hochstrasser, 2000; Pickart, 2001; Weissman, 2001). Ubiquitination is a major regulator of endocytosis and vesicular trafficking (Hicke, 2001; Raiborg et al., 2003). Ubiquitinated proteins are targeted to and regulate the vesicular trafficking machinery via interactions between the ubiquitin moiety and proteins that contain ubiquitin-binding domains (Harper and Schulman, 2006; Hicke et al., 2005; Hurley et al., 2006).

The ESCRT protein network targets ubiquitinated transmembrane proteins for degradation in the lysosome or yeast vacuole (Babst, 2005; Bowers and Stevens, 2005; Hurley and Emr, 2006; Slagsvold et al., 2006). These proteins were discovered in yeast, in which defects in their genes lead to an enlarged cargo-rich compartment adjacent to the vacuole (Bowers and Stevens, 2005). This phenotype is referred to as a class E vacuolar protein-sorting (VPS) defect. Yeast class E *VPS* genes encode the subunits of four hetero-oligomeric protein complexes: the Vps27/Hse1 complex (Bilodeau et al., 2003; Bowers and Stevens, 2005; Piper et al., 1995) and ESCRT-I, -II, and -III (Babst, 2005; Bowers and Stevens, 2005; Hurley and Emr, 2006; Slagsvold et al., 2006). The ESCRT network is conserved from yeast to human and sorts ubiquitinated transmembrane proteins into small vesicles that bud into the lumen of endosomes, thus forming multivesicular bodies (MVBs) (Gruenberg and Stenmark, 2004; Piper and Luzio, 2001). In mammalian cells, the ESCRT network directs the lysosomal degradation of signaling molecules such as the EGF receptor (Clague and Urbe, 2001; Haglund et al., 2003; Katzmann et al., 2002; Slagsvold et al., 2006). Further, this network is hijacked by viruses such as HIV, which use a process topologically equivalent to MVB formation to bud from cells (Demirov and Freed, 2004; Morita and Sundquist, 2004).

Vps27/Hse1 is a multifunctional complex required for MVB sorting of ubiquitinated cargo molecules as well as the efficient recycling of late Golgi proteins including the carboxypeptidase Y (CPY) sorting receptor, Vps10 (Bilodeau et al., 2002, 2003; Piper et al., 1995). Human Vps27 is known as Hrs (hepatocyte growth factor receptor substrate), and Hse1 has two human orthologs, STAM1 and STAM2 (signal-transducing adaptor molecule) (Komada and Kitamura, 2005) (Figure 1A). The Vps27/Hse1 and Hrs/STAM complexes sort cargo proteins from early endosomes to the ESCRT-I complex (Bilodeau et al., 2003; Katzmann et al., 2003) via clathrin-coated domains (Lloyd et al., 2002; Raiborg et al., 2002). The Vps27/Hse1 complex is targeted to early endosomes via the FYVE domains of Vps27 or Hrs (Raiborg et al., 2001), which bind to phosphatidylinositol 3-phosphate (PI(3)P). The Vps27/Hse1

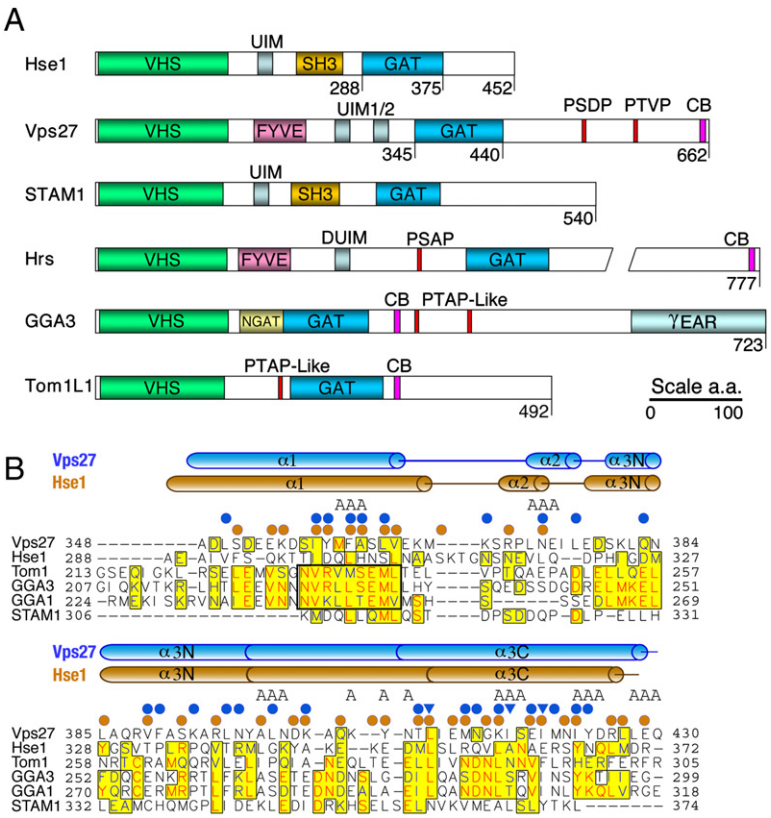

Figure 1. Modular Organization of Vps27, Hse1, and Related Proteins and Alignment of GAT Domains

(A) Modular organization of Vps27, Hse1, and other GAT-domain-containing proteins. Domain name abbreviations are as follows: VHS, Vps27/Hrs/STAM; UIM, ubiquitin-interacting motif; SH3, Src homology-3; GAT, GGA and TOM; GGA, Golgi-localized, γ-ear-containing, ADP-ribosylation-factor-binding protein; TOM, target of Myb; FYVE, Fab1/YOTP/Vac1/EEA1; CB, clathrin-binding; DUIM, double UIM; NGAT, the N-terminal region preceding the GAT domain, responsible for binding to Arf1-GTP; GAE, γ-adaptin ear. A helical region of Hrs is a putative, but unproven, GAT domain.

(B) GAT domains were aligned based on three-dimensional structural superposition where available (Vps27, Hse1, GGA1, GGA3, and Tom1), and otherwise by sequence homology with the most similar protein of known structure. Colored dots or triangles indicate residues of Vps27 (blue) and Hse1 (orange) that participate in the heterodimer interface. Residues shown in triangles were mutated in this study. The letter "A" above the alignment denotes residues of Vps27 mutated to Ala (Bilodeau et al., 2003). The major site 1 ubiquitin-binding motif of GGA1, GGA3, and Tom1 as discussed in the text is outlined in black.

complex recruits clathrin via a short peptide motif near the C termini of Vps27 and Hrs (Raiborg et al., 2002), and both proteins contain P(S/T)XP motifs that recruit ESCRT-I (Bilodeau et al., 2003; Katzmann et al., 2003; Lu et al., 2003).

The Vps27/Hse1 and Hrs/STAM complexes are scaffolds for binding of ubiquitinated cargo proteins and coordinating ubiquitination and deubiquitination reactions that regulate sorting. The yeast complex recruits ubiquitinated cargo via two tandem ubiquitin-interacting motifs (UIMs) in Vps27 (Bilodeau et al., 2002; Shih et al., 2002; Swanson et al., 2003) and one in Hse1. Hse1 and STAM isoforms recruit the deubiquitinating enzymes (DUBs) UBPY (Kaneko et al., 2003; Kato et al., 2000), AMSH (McCullough et al., 2006), and, in yeast, Ubp7 (Ren et al., 2007) through their SH3 domains. The Hse1 SH3 domain also recruits the adaptor protein Hua1, which, in turn, recruits a complex of the ubiquitin ligase Rsp5, the DUB Ubp2, and the regulatory protein Rup1 (Ren et al., 2007). There is a second mechanism in which the C terminus of Hse1 binds the ubiquitin ligase Rsp5 directly (Bowers et al., 2004; Ren et al., 2007). These mechanisms regulate different cargo to different extents. CPY sorting is slowed, but not blocked, when the complex is disrupted by the loss of Hse1 (Bilodeau et al., 2002). In contrast, cargo such as carboxypeptidase S (Cps1) and the mating factor receptor Ste3 are profoundly dependent on the integrity of the complex, and their sorting is largely blocked by loss of Hse1 (Bilodeau et al., 2002; Ren et al., 2007).

While much is known about individual domains of the Vps27/Hse1 complex, little is known about how the subunits of the complex associate with one another. A predicted coiled-coil region in the Vps27/Hse1 (Bilodeau et al., 2003) and Hrs/STAM (Mizuno et al., 2004) complexes is necessary for complex formation, and an adjacent region of STAM1 dubbed the "STAM-specific motif" (SSM) has also been implicated (Mizuno et al., 2004). To characterize the core around which the complex assembles, we carried out sequence-similarity searches in the region of the predicted coiled coil by using PSI-Blast (Altschul et al., 1997). To our surprise, these regions of Vps27, Hse1, and STAM all showed statistically significant similarity (E values of $\sim 10^{-9}$) to the GAT (GGAs and TOM) domains of the GGA and TOM trafficking adaptor proteins (Figures 1A and 1B). GAT domains are monomeric three-helix bundles (Collins et al., 2003; Shiba et al., 2003; Suer et al., 2003; Zhu et al., 2003) that bind to ubiquitin (Mattera et al., 2004; Puertollano and Bonifacino, 2004; Scott et al., 2004; Shiba et al., 2004). We sought to test the prediction that Vps27 and Hse1 contain GAT domains and to understand how a GAT domain-based core could assemble an oligomeric complex by determining the crystal structure of what we refer to as the Vps27/Hse1 core complex. The structure shows that the core complex consists of two intertwined GAT domains, each consisting of two helices from one subunit and one from the other. The two GAT domains are connected by a two-stranded coiled coil. Residues in the interface between the subunits

are shown to be essential for the normal sorting functions of these proteins. Finally, the role of the core in organizing the cooperative interactions of other domains of the Vps27/Hse1 complex was explored by using coarse-grained Monte Carlo simulations.

RESULTS

The Vps27/Hse1 Core Complex

Based on secondary structure predictions and the putative homology to known GAT domains, a protein construct comprising residues 345–440 of Vps27 fused to an N-terminal hexahistidine tag was coexpressed in *Escherichia coli* with a second untagged construct comprising residues 275–375 of Hse1. The Vps27 and Hse1 fragments coeluted from the chelating column and comigrated on size-exclusion chromatography (Figure 2A). All of the material consisted of the binary complex, and there was no observable population of free monomeric subunits. Since these portions of Vps27 and Hse1 are competent to form a highly stable binary complex, and there is no indication that other domains of these proteins are involved in complex formation, we refer to this complex as the "Vps27/Hse1 core complex" throughout the manuscript.

To determine the oligomeric state of the Vps27/Hse1 core complex in solution, the Vps27/Hse1 complex was analyzed by analytical ultracentrifugation. The global data analysis was consistent with a single ideal solute with a molecular mass of 23.2 ± 0.4 kDa. This compares well to the calculated molecular mass of 23,703 Da for a 1:1 complex of the Vps27 and Hse1 core fragments. The experimental stoichiometry of 1:1 heterodimers is n = 0.98 ± 0.02 (Figures 2B and 2C; Figure S1, see the Supplemental Data available with this article online). The core region of Hse1 expressed alone was too unstable to characterize by analytical ultracentrifugation. The isolated core region of Vps27 was found to be relatively stable, however. The isolated core region of Vps27 was characterized by sedimentation equilibrium experiments (Figure 2D). The global data analysis in terms of a single ideal solute resulted in poor data fits, but analysis in terms of two noninteracting solutes returned excellent fits consistent with the presence of monomeric Vps27 and a higher-molecular mass species (Figure 2D; Figure S2). The best fit showed that the isolated Vps27 core sample contained 94% monomer and 6% aggregate on a molar basis.

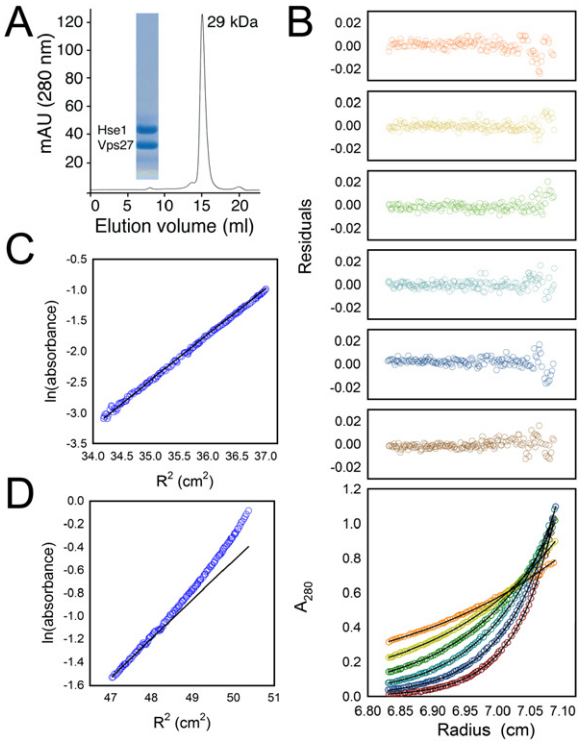

Figure 2. Hydrodynamic Properties of the Vps27/Hse1 Core Complex

(A) Gel filtration analysis of the recombinant Vps27/Hse1 core showing comigration at an apparent mass of 29 kDa. This is slightly higher than the calculated mass of 23.2 kDa for a 1:1 complex, and is therefore consistent with an elongated 1:1 complex, but is not consistent with any oligomer with a greater number of subunits.

(B) Sedimentation equilibrium profiles at 4.0°C plotted as a distribution of the absorbance at 280 nm versus r at equilibrium. Data were collected at 13 (orange), 16 (yellow), 19 (green), 22 (cyan), 25 (blue), and 28 (brown) krpm at a loading A_{280} of 0.75. The solid lines show the best-fit global analysis (carried out for the three loading concentrations) in terms of a single ideal solute; the corresponding residuals are shown in the panels above the plot.

(C) Sedimentation equilibrium profile at 4.0°C and 22 krpm plotted in terms of $\ln A_{280}$ versus r^2. The data shown correspond to a loading A_{280} of 0.25. The solid line indicates the plot expected for a monodisperse 1:1 Vps27:Hse1 complex.

(D) Sedimentation equilibrium profile of the Vps27 core region in isolation at 4.0°C and 22 krpm plotted in terms of $\ln A_{280}$ versus r^2. The data shown correspond to a loading A_{280} of 0.60. The solid line indicates the plot expected for a monomeric Vps27, indicating the presence of higher oligomers.

Structure of the Vps27/Hse1 Core Complex

The crystal structure of the Vps27/Hse1 core complex was determined at 3.0 Å resolution by a two-wavelength multiwavelength anomalous dispersion experiment at the Se edge (Figure 3A). The overall structure is barbell like, with dimensions of roughly 90 × 20 × 20 Å (Figures 3B and 3C). The structures of the two subunits are very similar to each other, with an rmsd of 1.8 Å for the overlay of 67 Cα atoms. The two subunits are intimately intertwined such that 2104 $Å^2$ of solvent-accessible surface area is buried per subunit (Figures 3D and 3E). The N termini of the subunits are close together (17 Å apart) at the middle of the barbell. In contrast, the C termini are at opposite ends of the barbell, 87 Å away from each other.

Each subunit consists of three α helices. At 89 and 72 Å, respectively, the α3 helices are the longest in the structure. The α3 helices have three distinct structural roles. The N- and C-terminal portions of α3 contribute to the formation of three-helix bundles at each end of the barbell. One bundle (HHV) consists of α1 (residues 288–312) and α3-N (322–341) of Hse1, together with α3-C of Vps27 (410–438). The second bundle (VVH) consists of α1 (residues 351–371) and α3-N (381–399) of Vps27, together

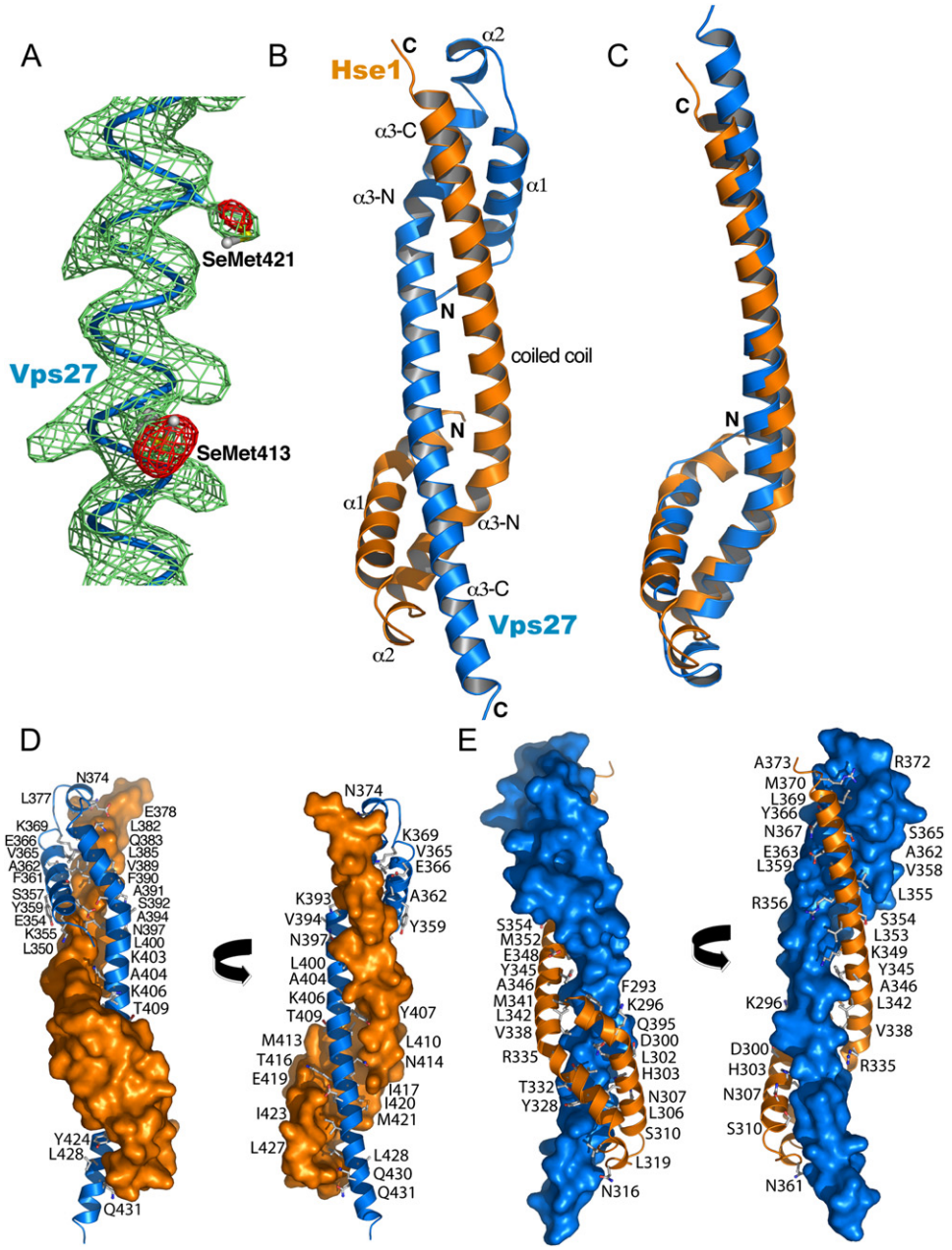

Figure 3. Crystal Structure of the Vps27/Hse1 Complex

(A) Density-modified MAD Fourier synthesis (green) contoured at 1.0σ and Se anomalous difference Fourier (red) contoured at 4.0σ superimposed on the refined structure; SeMet residues are highlighted.

(B) Overall structure of the core heterodimer; Vps27 is blue, and Hse1 is orange.

(C) Superposition of the core portions of the Vps27 and Hse1 monomers.

(D) Surface of Hse1 showing interactions with labeled residues of Vps27.

(E) Surface of Vps27 showing interactions with labeled residues of Hse1.

with α3-C of Hse1 (354–372). The narrow center of the barbell consists of a two-stranded coiled coil formed by the central portion of each α3 helix. The coiled-coil region spans residues 396–414 of Vps27 and 338–356 of Hse1. Several residues of the coiled coil are thus also part of the helical bundles.

Domain-Swapped GAT Domains in Vps27 and Hse1

The two three-helix bundles closely resemble the structures of GAT domains (Figures 4A and 4B). A search of the structural database with Dali (Holm and Sander, 1995), using the HHV bundle as the probe structure, identified the GAT domain of Tom1 (Akutsu et al., 2005) as the

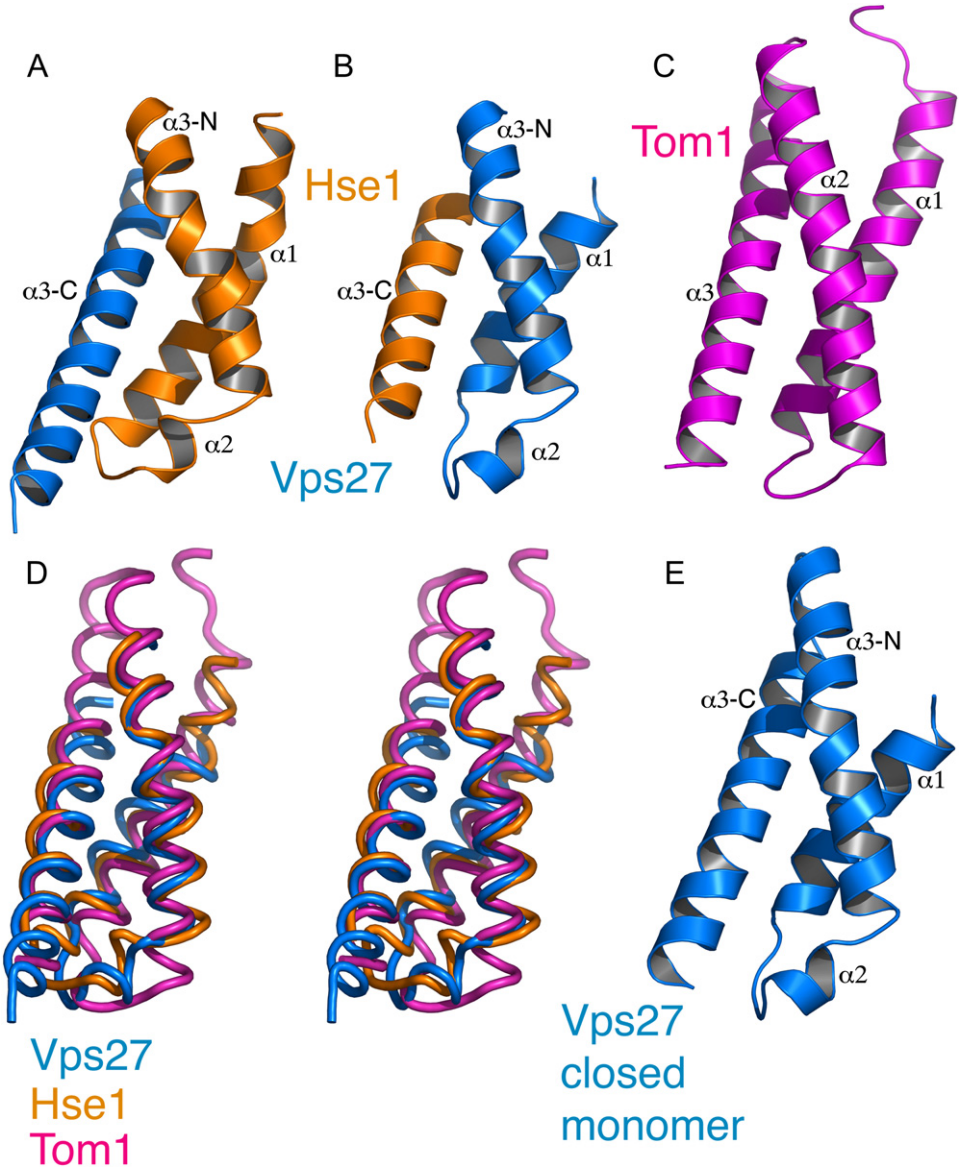

Figure 4. GAT Domains in Vps27 and Hse1

(A) The HHV helical bundle.

(B) The VVH helical bundle.

(C) The GAT domain of Tom1 shown in the same orientation as in (A) and (B).

(D) Superposition of the HHV and VVH bundles and the Tom1 GAT domain.

(E) Model for the closed monomeric conformation of the Vps27 GAT domain, generated by superimposing the Vps27 structure on the Tom1 GAT domain monomer.

top-scoring match, with a Z score of 7.7 (Figure 4C). The Tom1-GAT domain overlays the HHV bundle with an rmsd of 2.6 Å over 73 Cα positions. The VVH bundle overlays with an rmsd of 2.2 Å over 47 Cα positions. These rmsd values compare to values of 1.6–1.8 Å over 86–90 Cα positions for superpositions of the structures of GAT domains of GGA1, GGA3, and Tom1 with each other. Given the significant sequence and structural similarity, it seems appropriate to designate the Vps27/Hse1 three-helix bundles as members of the GAT domain family (Figures 1A and 1B). The α3-N segment corresponds to α2 of the GAT domain, and α3-C of the opposing subunit corresponds to α3 of the GAT domain. The major difference between the GAT domains of Vps27/Hse1 compared to GGAs and Tom1 is that the former are heterodimeric, whereas the latter are monomeric. Further, the Vps27/Hse1 GAT domains contain a very short helix, α2 (Figures 4A and 4B), which has no counterpart in the GGA GAT structures.

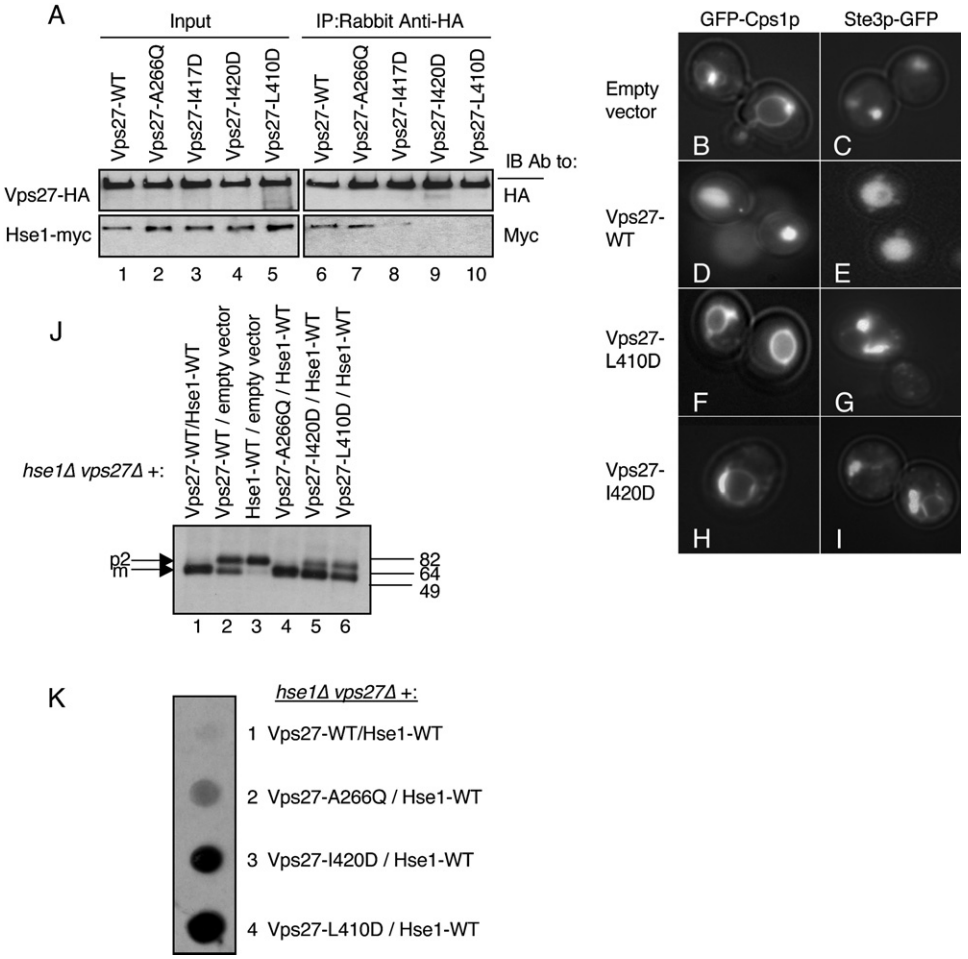

Figure 5. The Vps27/Hse1 Interface Is Required for Sorting

(A) Expression levels and coimmunoprecipitation of HA-tagged Vps27 and myc-tagged Hse1 proteins. Left panels. Whole-cell lysates from *vps27Δ hse1Δ* cells cotransformed with Hse1-myc and Vps27-HA constructs were lysed and subjected to SDS-PAGE and immunoblot analysis with anti-HA and anti-myc antibodies. Right panels. Rabbit anti-HA immunoprecipitation from the above-described lysates, followed by SDS-PAGE and immunoblotting with mouse anti-HA and mouse anti-myc antibodies.

(B–I) Fluorescence microscopy images of GFP chimeras of Ste3 and Cps1 in *vps27Δ* cells expressing Vps27-WT or the indicated core-complex mutants.

(J) CPY maturation in *vps27Δ hse1Δ* cells expressing various constructs. Cells were metabolically labeled with ^{35}S-metionine for 10 min (pulse) and chased for 15 min in complete medium, and endogenous CPY was immunoprecipitated with anti-CPY antibody. The 15 min point samples were analyzed by SDS-PAGE followed by fluorography.

(K) CPY colony blot assay on *vps27Δ hse1Δ* cells coexpressing Hse1-WT and various Vps27 constructs. Colonies from each strain were spotted onto selective medium and overlayed with nitrocellulose. Secreted CPY was detected by immunoblotting the nitrocellulose with an anti-CPY antibody.

Mutational Analysis of the Heterodimer Interface

To confirm the physiological importance of the subunit contacts observed in the Vps27/Hse1 core-complex crystal structure, point mutations were introduced into the heterodimer interface. Vps27 residues Leu410, Ile417, and Ile420 are deeply buried in the dimer interface (Figure 3E) and were selected for mutagenesis to the charged residue Asp. The mutations were introduced into a full-length HA-tagged Vps27 construct to generate the mutants Vps27-I417D, Vps27-I420D, and Vps27-L410D. For comparison, a UIM mutation (Vps27-A266Q) that was predicted not to abolish core-complex assembly was also generated. These point mutants, as well as wild-type (WT) HA-tagged Vps27 (Vps27-WT), were coexpressed with wild-type Hse1-myc in *vps27Δ hse1Δ* yeast cells. To determine the expression levels of these proteins, whole-cell lysates from these strains were subjected to SDS-PAGE and immunoblot analysis with antibodies to the HA and myc epitopes. No significant difference in expression level was detected among Vps27-WT, core-complex mutants, or the Vps27-A266Q mutant (Figure 5A, lanes 1–5). Hse1-myc levels in each strain were also equivalent. The lysates were then subjected to immunoprecipitation with anti-HA antibody and were analyzed by immunoblotting with anti-HA and anti-myc antibodies. As expected, Hse1-myc protein coimmunoprecipitated with both Vps27-WT and the

UIM mutant, Vps27-A266Q (Figure 5A, lanes 6 and 7); however, this interaction was abolished by all three core-complex mutations (Figure 5A, lanes 8–10).

We next sought to determine the functional consequence of core-complex mutations. MVB sorting was tested by using GFP chimeras of the biosynthetic cargo protein Cps1 (GFP-Cps1) and the plasma membrane receptor Ste3 (Ste3-GFP) expressed in *vps27Δ* cells. Both GFP-Cps1 and Ste3-GFP accumulated in the class-E compartment in *vps27Δ* cells expressing only empty vector (Figures 5B and 5C). In addition, GFP-Cps1 labeled the limiting membrane of the vacuole (Figure 5B). Transformation of the *vps27Δ* strain with Vps27-WT restored transport of both cargo proteins into the lumen of the vacuole (Figures 5D and 5E). In contrast, neither of the core-complex mutants, Vps27-L410D or Vps27-I420D, was capable of restoring this transport (Figures 5F–5I).

To assess the sorting of the soluble vacuolar hydrolase CPY, the proteolytic maturation of the Golgi precursor (p2) form to the vacuolar mature (m) form was examined by pulse-chase analysis of *vps27Δ hse1Δ* cells transformed with various Vps27 and Hse1 constructs (Figure 5J). After a 15 min chase period, CPY species were isolated by immunoprecipitation and were analyzed by SDS-PAGE (Figure 5J). *vps27Δ hse1Δ* cells coexpressing Vps27-WT and Hse1-WT exhibited normal CPY maturation, and the majority of the hydrolase migrated as mature CPY (Figure 5J, lane 1). Significant differences were observed in CPY maturation in *vps27Δ hse1Δ* cells expressing either Vps27-WT alone or Hse1-WT alone (Figure 5J, lanes 2 and 3). Specifically, cells expressing Vps27-WT alone (Figure 5J, lane 2) exhibited a partial CPY-maturation defect, as compared to cells expressing Hse1-WT alone (Figure 5J, lane 3), in which virtually all of the CPY migrated as the p2 form. These findings are consistent with past results that Vps27 is essential for CPY maturation, while loss of Hse1 results in only a modest reduction in CPY processing (Bilodeau et al., 2002). Interestingly, none of the core-complex mutants (Vps27-I420D and Vps27-L410D shown) fully complemented the loss of Vps27 in *vps27Δ hse1Δ* cells expressing Hse1-WT alone (Figure 5J, lanes 5 and 6), while Vps27-A266Q behaved identically to Vps27-WT (Figure 5J, lane 4). Similar results were obtained when the effects of the Vps27-A266Q and core-complex mutations were analyzed in a CPY secretion colony blot assay (Figure 5K). In this assay, secreted CPY was undetectable in *vps27Δ hse1Δ* cells expressing Vps27-WT, and it was barely visible in *vps27Δ hse1Δ* cells expressing Vps27-A266Q (Figure 5K, lanes 1 and 2); however, significant amounts of CPY secretion were detected in *vps27Δ hse1Δ* cells expressing either Vps27-I420D or Vps27-L410D (Figure 5K, lanes 3 and 4). These data are also consistent with previous studies showing no significant role for the UIM of Vps27 in CPY maturation (Bilodeau et al., 2002). These results thus show that point mutants in Vps27 that abrogate binding to Hse1 affect CPY sorting to roughly the same extent as the deletion of the Hse1 gene. Taken together with the results showing that these mutants block sorting of Cps1 and Ste3, these data demonstrate that the Vps27-interface residues observed in the crystal structure are important for the cellular functions of the Vps27/Hse1 complex.

Monte Carlo Simulation Analysis of the Properties of the Vps27/Hse1 Complex

The Vps27/Hse1 core is the last folded domain of the Vps27/Hse1 complex to have its three-dimensional structure solved. The complex consists of several folded domains linked by unstructured segments (Figure 6). This structural information allowed us to conduct a theoretical analysis of the organization, dynamics, and interactions of this complex with the model ubiquitinated transmembrane cargo, Cps1 (Ub-Cps1), by using a coarse-grained Monte Carlo (MC) approach. The UIMs of Vps27 and Hse1 were modeled as interacting with ubiquitin moieties on Lys8 of the Cps1 cytosolic tail (Katzmann et al., 2001). The distance distributions of all three Ub-Cps1 molecules to a noninteracting domain used as a reference point are found to be equivalent over the course of the simulation, indicating that the system is well sampled and thoroughly equilibrated (Figure 7A).

The MC simulations showed this complex to be flexible and dynamic, capable of binding multiple ubiquitin moieties situated at different distances from the membrane. Even with the overall topology maintained, the Vps27/Hse1 complex can undergo large conformational changes, as indicated by the time series and distributions of distances between nonspecifically interacting domains (Figures 7B and 7C). Along the MC simulation trajectories, the Vps27/Hse1 core retains an extended and open configuration with a radius of gyration, R_g, between ~40 and ~60 Å (Figures 7D and 7E). A globular protein of the same molecular weight as the simulated portion of Vps27/Hse1 would be expected to be much more compact, with an R_g of ~28 Å.

Interactions of the Vps27 FYVE domain with PI(3)P and the two Vps27 UIM domains with Ub-Cps1 keep this contiguous portion of the Vps27 complex near the membrane (Figure 7F). Unlike the two Vps27 UIM domains, the single Hse1 UIM does not directly adjoin a membrane-binding domain in the primary sequence. Therefore, on average, the Hse1 UIM is found farther from the membrane (Figure 7F). To explore the relative contributions of the different UIMs to overall binding on the membrane, the fraction of Ub-Cps1 molecules bound to the three different UIMs in isolation, in the full Vps27/Hse1 complex, and in Vps27 alone were calculated as a function of concentration (Figure 7G). The affinities of the Vps27 UIMs in the context of the full complex are comparable to those of the isolated UIMs. In contrast, the affinity of the Hse1 UIM for Ub-Cps1 is substantially reduced in the complex. Several factors contribute to the difference. Within the complex, Ub-Cps1/UIM binding is limited by steric restrictions and internally competitive interactions that are not present for the isolated UIM. This negative steric contribution to binding is balanced by cooperative interactions with the membrane and membrane-bound Ub-Cps1 molecules. This positive cooperative contribution is stronger for

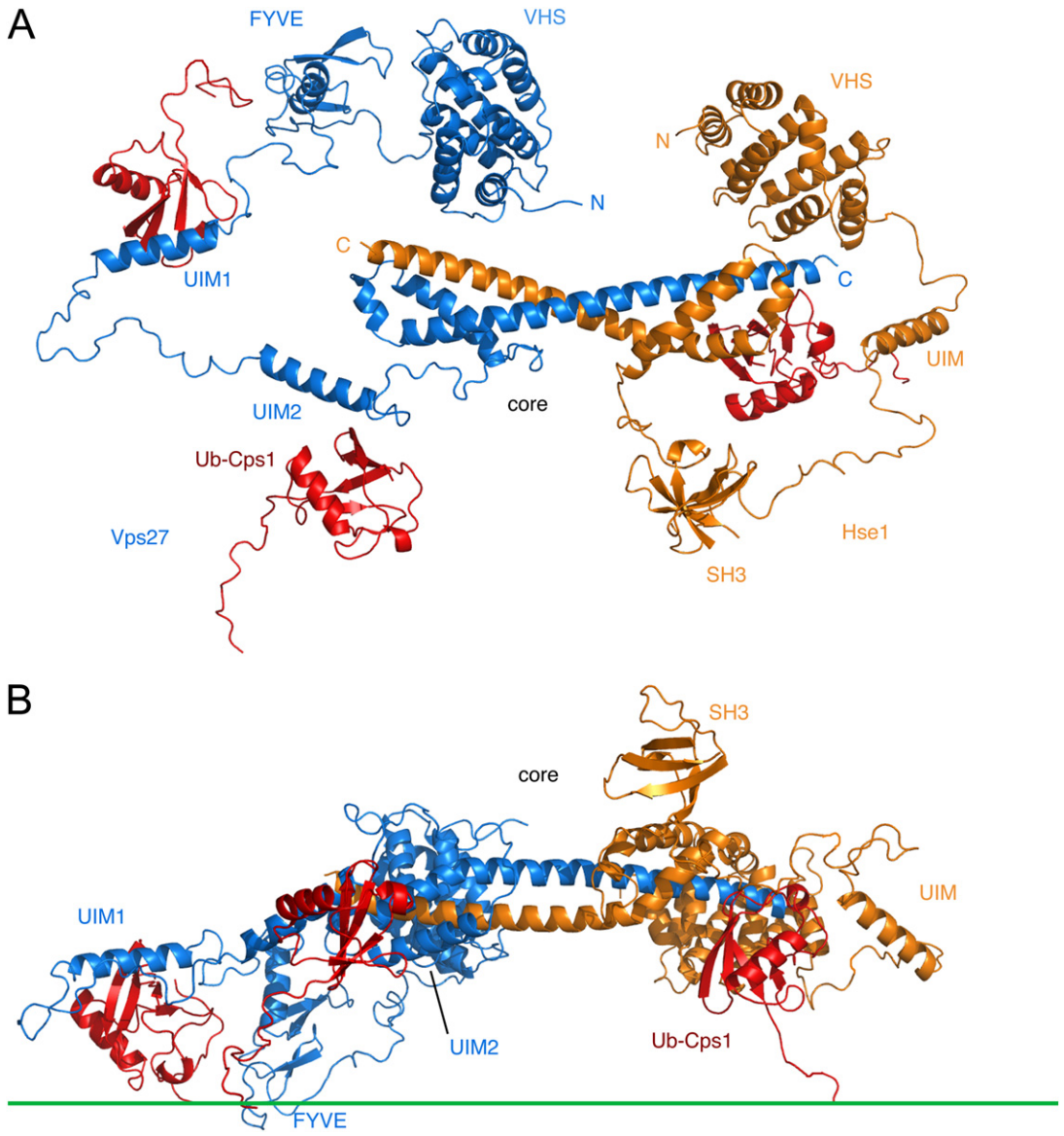

Figure 6. A Unified Model for the Interaction of Vps27/Hse1 with Membranes and Ubiquitinated Cargo

(A and B) The figure shows a single snapshot from the MC simulation. (A) View looking directly down toward the membrane. (B) View normal to the plane of the membrane (the membrane surface is indicated by the green line). Vps27 is shown in blue, Hse1 is shown in orange, and ubiquitinated cargo is shown in red.

Vps27 than for Hse1 because the FYVE domain and two UIMs of Vps27 are close together. Therefore, the Vps27 UIM domains appear to have much stronger interactions with Ub-Cps1 than the Hse1 UIM.

DISCUSSION

The structure of the Vps27/Hse1 core fills the last major gap in our understanding of the organization of this complex and led us to several unexpected observations. First, the region involved in forming the core is more extensive than anticipated and extends beyond the predicted coiled-coil regions in both the N- and C-terminal directions. Second, the core contains two GAT domains. Third, the core assembles by the interchange of the homologous C-terminal halves of the α3 helices from each GAT domain. In addition, the resolution of this structure has allowed us to model its function as a scaffold for ubiquitin-binding and ubiquitination-deubiquitination reactions at the endosomal membrane.

The interchange of the homologous α3 C-terminal halves from Vps27 and Hse1 is reminiscent of the mechanism of "domain swapping." As originally defined, domain swapping refers to the oligomerization of identical protomers by interchange of identical regions of subunits (Liu

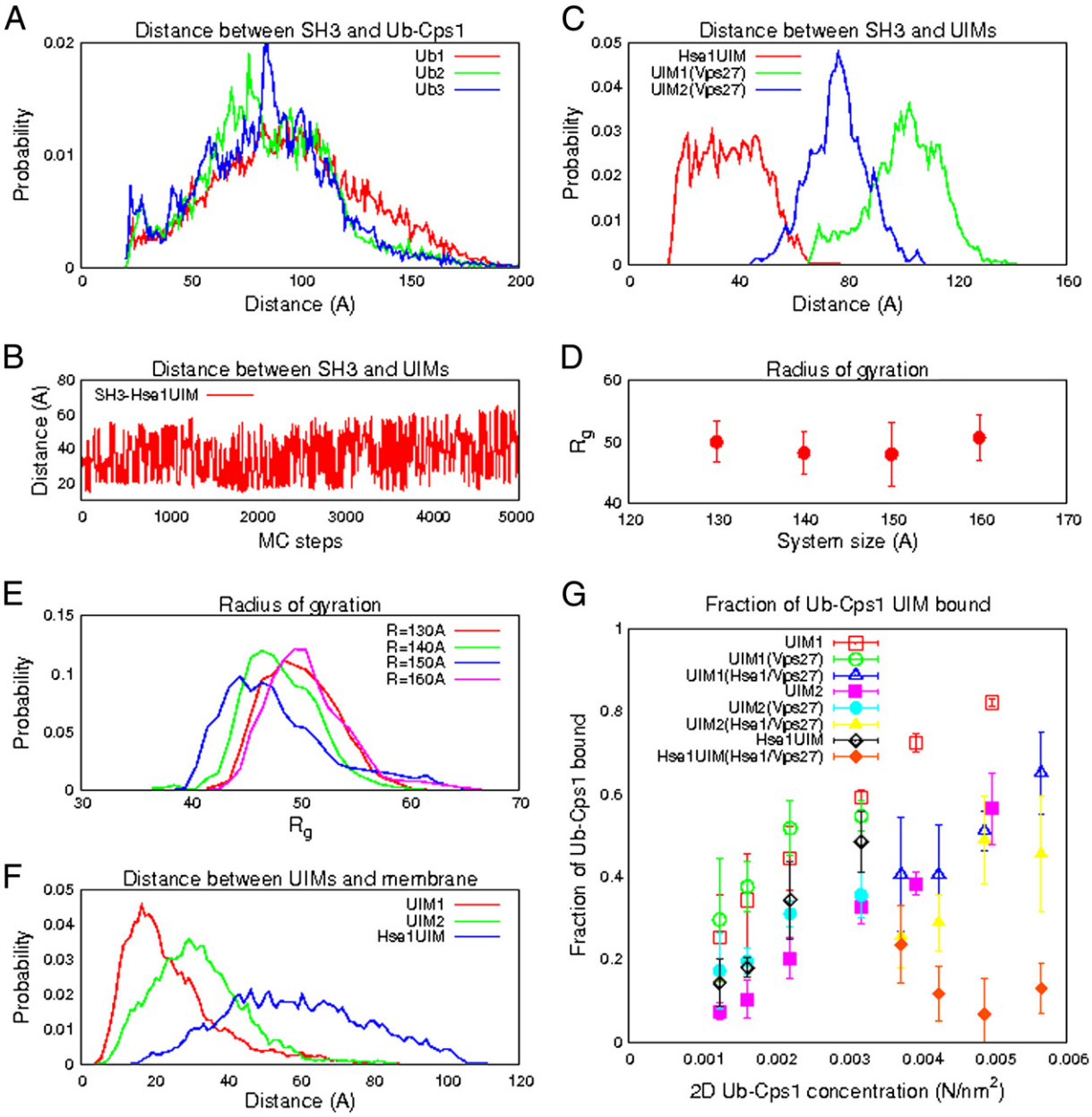

Figure 7. Dynamics of the Vps27/Hse1 Complex

(A) Distributions of the distances between the SH3 domain and three Ub-Cps1 molecules.

(B) Time series of the distance between the SH3 domain and the Hse1 UIM.

(C) Distributions of the distances between the SH3 domain and three UIMs.

(D) Average of R_g as a function of the overall system size.

(E) Distributions of R_g for different system sizes.

(F) Distributions of the distances between three UIMs and the membrane surface.

(G) Fraction of Ub-Cps1 bound to the different UIMs (in isolation, on Vps27 alone, and on the full Vps27/Hse1 complex) as a function of the two-dimensional Ub-Cps1 concentration in the membrane.

and Eisenberg, 2002). The assembly of the Vps27/Hse1 core seems to us structurally and functionally equivalent to domain swapping in every respect other than the sequence identity of the exchanged regions.

In order to judge whether the domain-swapped complex represents the bona fide assembly mechanism for Vps27 and Hse1 in vivo, we analyzed the structure in the light of mutational analysis in the literature, and we carried out additional mutational studies of complex formation. Residues 416–418 of Vps27 (sequence KIS) were critical for complex formation with Hse1 (Bilodeau et al., 2003). Vps27 Ile417 within this sequence is deeply buried and

almost completely surrounded by hydrophobic residues from Hse1 (Figure 3), consistent with a critical role in function. We mutated Vps27 residues Leu410, Ile417, and Ile420 individually to Asp, and we found that these mutations prevented formation of the complex with Hse1. For each cargo tested, Cps1, Ste3, and CPY, these mutations resulted in a loss of function mirroring that seen in the deletion of Hse1. This establishes that the protein:protein interface observed in the structure is responsible for the assembly of the Vps27/Hse1 complex in yeast.

Despite the fact that Vps27 and Hse1 are subunits of a tightly assembled heterodimer, deletion of the gene encoding each subunit results in a quantitatively different defect in cargo sorting. Deletion of *VPS27* causes a much stronger CPY-missorting phenotype than deletion of *HSE1* (Bilodeau et al., 2002) (also see Figure 5). The missorting of Cps1 and Ste3 is also more severe in *VPS27*- than *HSE1*-deletion mutants (Bilodeau et al., 2002). *HSE1*-disruption phenotypes are more manifest in certain genetic backgrounds, like that of the SF8389D yeast strain used in these studies (Bilodeau et al., 2002). Our observations shed light on the probable cause for these phenotypic differences. Although the Vps27 core domain prefers to assemble as a heterodimer with the Hse1 core domain, it is nonetheless stable as a monomer when expressed in the absence of the Hse1 core domain. This is likely due to its ability to form an intramolecular GAT fold. In contrast, the Hse1 core domain expressed in isolation tends to aggregate and be degraded. Deletion of the *VPS27* gene may thus lead to loss of both the Vps27 and Hse1 proteins, whereas deletion of the *HSE1* gene would still leave enough Vps27 protein to sustain a modicum of function. In addition, Vps27 contains the main determinant of attachment of the complex to membranes, the FYVE domain, such that monomeric Hse1 is likely incapable of efficient recruitment to endosomes. Conversely, monomeric Vps27 could bind to membranes independently of Hse1, thus bringing its ubiquitin-, ESCRT-I-, and clathrin-binding activities to bear on MVB sorting. Finally, the MC simulations show that the two UIM domains of Vps27 are closer to the membrane and exhibit more cooperativity than the single UIM domain of Hse1.

The human Hrs/STAM complex has been intensively studied, but the structural basis for its assembly remains unknown. The significant sequence homology between STAM, Hse1, and Vps27 allows us to predict that the core region of STAM will adopt the same structural fold as Vps27 and Hse1. The so-called SSM, which is needed for Hrs/STAM complex formation (Mizuno et al., 2004), corresponds to the C-terminal half of helix α1 and a few residues immediately following α1. Several of the conserved residues in the SSM correspond to key hydrophobic anchor residues in the subunit interface. The sequence of the core region of Hrs diverges from those of Vps27, Hse1, and STAM. However, the region of Hrs corresponding to the Vps27 GAT domain is predicted to be α-helical. Further, the examples of Vps27 and Hse1 suggest that the STAM GAT domain requires a complementary GAT domain in Hrs with which to associate.

The unexpected observation of GAT domains in Vps27 and Hse1 highlights the parallel roles of these proteins with other GAT-domain-containing trafficking adaptors, the GGAs and Tom1 and Tom1-like proteins. The GGAs are modular proteins that contain a receptor-binding VHS domain; an Arf-binding helical hairpin domain; a ubiquitin-, Rabex-5, and ESCRT-I-binding GAT domain; an unstructured region containing autoinhibitory and clathrin-binding domains; and a GAE domain that binds to various accessory proteins (Bonifacino, 2004). Tom1 and its relatives Tom1L1 and Tom1L2 have similar modular structures to the GGAs (Figure 1A), and they bind to ubiquitin via their GAT domains (Katoh et al., 2004; Yamakami et al., 2003) and to ESCRT-I (Puertollano, 2005). Collectively, the GGAs, Tom1, and the Tom1-like proteins and the Vps27/Hse1 and Hrs/STAM complexes comprise a class of endosomal clathrin-binding proteins that sort ubiquitinated cargo proteins into the ESCRT pathway (Raiborg et al., 2006). These similarities highlight the GAT domain proteins collectively (Figure 1A) as a family of proteins that sort ubiquitinated cargo into the ESCRT system.

The GAT domains of GGA1, GGA3, and Tom1 bind ubiquitin (Katoh et al., 2004; Puertollano and Bonifacino, 2004; Scott et al., 2004; Shiba et al., 2004) with affinities ranging from 180 to 410 μM (Akutsu et al., 2005; Kawasaki et al., 2005; Prag et al., 2005). However, no ubiquitin binding to the Vps27/Hse1 core was detected by isothermal titration calorimetry or surface plasmon resonance at concentrations of up to 8.0 mM and 2.0 mM, respectively (data not shown). Known ubiquitin-binding GAT domains contain two ubiquitin-binding sites. Ubiquitin binds to the GGA and Tom1 GAT domains at site 1 on helices α1 and α2 and site 2 on helices α2 and α3. These sites are incompletely conserved in Vps27 and Hse1 (Figure 1B). Unlike Vps27 and Hse1, the GGAs and Tom1 do not contain ubiquitin-binding UIMs. If the family of GAT-domain-containing adaptors evolved from a common ancestor, the GAT domains have served multiple purposes in ubiquitin binding, dimerization, and other functions. By the same token, different ubiquitin-binding, GAT-domain-containing proteins acquired different mechanisms for binding ubiquitinated cargo, some binding through the GAT domain, and others via their UIMs.

The structures and the ubiquitin and membrane affinities of individual domains from the Vps27/Hse1 and Hrs/STAM complexes are known (Diraviyam et al., 2003; Fisher et al., 2003; Hirano et al., 2006; Kaneko et al., 2003; Mao et al., 2000; Misra and Hurley, 1999; Stahelin et al., 2002; Swanson et al., 2003). Despite a wealth of information on individual domains, it has not been possible to integrate this knowledge into a unified model of the Vps27/Hse1 complex. The structure determination of the Vps27/Hse1 core provides the missing link that allows for the integration of the domain. The simulations show that cooperativity between the Vps27 and FYVE and UIM domains in membrane and ubiquitinated membrane protein binding offsets steric constraints imposed in the complex. The simulations portray the complex as open

and dynamic. Vps27/Hse1 traffics a variety of ubiquitinated cargo. The molecular weight, the size of the cytosolic domain, and the location of the ubiquitination sites on these cargoes vary widely. An open, dynamic complex such as Vps27/Hse1 can adapt to these differences in cargo in ways that a rigid complex could not. Finally, the simulations show that the Hse1 SH3 domain, which targets DUBs that potentially deubiquitinate cargo, samples conformational space that frequently approaches within 20 Å of ubiquitinated cargo. This suggests that the action of the Hse1 UIM and SH3 domains coordinates ubiquitinated cargo-binding and deubiquitination reactions.

A model has been proposed for Hrs, based on a 16 Å resolution cryo-EM structure of an Hrs hexamer determined in the absence of STAM (Pullan et al., 2006). In the Hrs model, three sets of membrane and ubiquitin-binding domains are located 175 Å apart from each other at two sets of end caps. It is difficult to compare these models given the substantial differences in the Hrs and Vps27 core sequences and the presence of a 1:1 heterodimer in one structure versus a homohexamer in the other.

The core of the Vps27/Hse1 complex contains an elegant variation on the GAT domain, which does not bind ubiquitin directly, but instead coordinates ubiquitinated cargo-binding and ubiquitination and deubiquitination reactions. The structure of the Vps27/Hse1 complex shows how the complex can spatially confine ubiquitinated cargo and coordinate the action of DUBs (e.g., Ubp7) against a tightly localized subpopulation of substrate. Such a mechanism could help account for the biological specificity of this DUB, given the large number of potential substrates in the cell. Most importantly, the structure of the Vps27/Hse1 core complex has provided us with a unifying framework for understanding the integrated action of the many modular domains of these two proteins.

EXPERIMENTAL PROCEDURES

Protein Expression, Purification, and Crystallization

DNA sequences encoding Vps27 and Hse1 genes were amplified by PCR from *Saccharomyces cerevisiae* genomic DNA. DNA coding for residues 345–440 of Vps27 was subcloned in frame with a hexahistidine tag followed by a TEV protease cleavage sequence into the pST39 (Tan, 2001) expression vector. DNA coding for residues 275–375 of Hse1 was subsequently cloned into the same vector without a tag to yield a polycistronic expression vector for the Vps27/Hse1 core complex (pHisVps27/Hse1). The Hse1 GAT domain with similar boundaries was cloned into pHIS-Parallel.2 in frame to an N-terminal His tag and a TEV recognition site. Site-directed mutagenesis of pHisVps27/Hse1 was performed by using the QuikChange kit (Stratagene) with appropriate DNA primers, and the entire sequences were verified by DNA sequencing.

The individual GAT domains of Vps27 or Hse1 were overexpressed in *Escherichia coli* BL21 (λDE3) Rosetta cells (Novagen) overnight at 20°C with 1 mM IPTG. Pellets were resuspended in 0.5 M NaCl, 10% glycerol, and 50 mM Tris-HCl (pH 8.0) supplemented with protease inhibitors. Cells were disrupted by lysozyme treatment, followed by sonication and centrifugation. The proteins were then purified on a Ni-NTA agarose column. The His tags were removed by cleavage with TEV protease, and the samples were passed through a second Ni-NTA column, followed by gel filtration. The Vps27/Hse1 core complex was overexpressed and purified in the same manner. The selenomethionyl form of the complex was expressed in the methionine auxotroph *E. coli* strain B834 (λDE3) grown in defined media that contained selenomethionine and was purified as described above.

The native and selenomethionyl forms of the Vps27/Hse1 core complex were concentrated to 18 mg/ml and were crystallized in 1.1–1.4 M ammonium sulfate, 0.1 M Tris-HCl (pH 8.85) in hanging drops at a 1:1 ratio of protein:precipitant. Crystals were improved by microseeding into similar conditions with 1.25 M ammonium sulfate. Individual crystals were cryoprotected with Paratone-N (Hampton Research) and were frozen in liquid nitrogen.

Structure Determination

A two-wavelength MAD data set was collected from a single selenomethionyl crystal at the Advanced Photon Source (APS) synchrotron, Argonne National Laboratory at 95 K. Energies for the MAD experiment were chosen at the inflection point and remote at 12,658 and 12,750 eV, respectively. Data were analyzed with DENZO and Scalepack (HKL Research). Eight selenium atoms were located by a direct methods search with SnB (Weeks and Miller, 1999), and phases were calculated by using Phasit (Furey and Swaminathan, 1997). Density modification of the initial maps was performed by using RESOLVE (Terwilliger, 2000), DM, and Solomon of the CCP4 suite of programs (CCP4, 1994). The resulting maps were used to build atomic models in O (Jones et al., 1991) and Coot (Emsley and Cowtan, 2004). The model was then refined with CNS (Brunger et al., 1998) (Table 1) at 3.0 Å against the inflection point data set.

Gel Filtration

In vitro analysis of the oligomeric state of purified recombinant GAT domains from the individual proteins and from the complex was performed on a Superdex 200 HR 30/10 column (Amersham Pharmacia Biotech) in 150 mM NaCl, 50 mM Tris-HCl (pH 8.0).

Sedimentation Equilibrium

Sedimentation equilibrium experiments were conducted at 4.0°C on a Beckman Optima XL-A analytical ultracentrifuge. Samples in 50 mM Tris (pH 8.0) were loaded at concentrations corresponding to measured A_{280} values of 0.25, 0.50, and 0.75. Data were acquired at 13, 16, 19, 22, 25, and 28 krpm as an average of 4 absorbance measurements at 280 nm and a radial spacing of 0.001 cm. Equilibrium was achieved within 48 hr. Data were analyzed globally in SEDPHAT 4.3 (Schuck, 2003) (http://www.analyticalultracentrifugation.com/sedphat/sedphat.htm) by using solution densities (ρ) and protein partial specific volumes (ν) calculated in SEDNTERP (J. Philo; http://www.jphilo.mailway.com/) as described in the text. Excellent fits were observed in all cases. For the sample consisting of the Vps27 core region alone, the mass of the smallest species was fixed to that expected for the monomer to return a value of 48 kDa for the oligomeric species (n = 4.3). This higher-mass species contributes ~20% of the total absorbance; therefore, a solution with an absorbance at 280 nm of 1.0 will contain 130 μM of the monomer and 9 μM of the aggregate, demonstrating that the Vps27 monomer is the major species.

Coimmunoprecipitation

Twenty OD_{600} of cells grown to midlog phase were lysed in TBS-T (10 mM Tris, 140 mM NaCl, 0.1% Tween 20 [pH 7.5]) supplemented with protease inhibitor cocktail (Roche, Indianapolis, IN) by using glass bead lysis. Lysates were centrifuged at 14,000 rpm at 4°C, and supernatants were precleared by incubation for 60 min at 4°C with 30 μl Protein A-Sepharose beads (Amersham Pharmacia Biotech, Piscataway, NJ) and centrifugation at 8,000 × g for 5 min. The precleared lysates were incubated for 2 hr at 4°C with 30 μl Protein A-Sepharose beads bound to rabbit polyclonal anti-HA antibody (Covance, Princeton, NJ). The beads were then washed four times with TBS-T and subjected to SDS-PAGE and immunoblotting analysis with either mouse monoclonal anti-HA or mouse monoclonal anti-myc (9E10) (Covance, Princeton, NJ).

Table 1. Crystallographic Data Processing, Phasing, and Refinement Statistics

Collection Energies	Inflection	Remote
Data Processing		
Wavelength (Å)	0.97948	0.97242
Space group	$P3_221$	$P3_221$
Cell dimensions		
a, b, c (Å)	62.4, 62.4, 94.5	62.4, 62.4, 94.6
α, β, γ (°)	90, 90, 120	90, 90, 120
Resolution (Å)	3.0	3.2
I/σI	18.1 (2.5)	12.7 (0.4)
Redundancy	4.1 (2.3)	3.7 (1.2)
Completeness (%)	97.5 (88.1)	82.5 (17.3)
Number of reflections	4415	3798
R_{sym}	0.052 (0.336)	0.059 (0.744)
Refinement		
Resolution (Å)	3.0	
R_{work}/R_{free}	0.22/0.28	
Number of protein atoms	1429	
Number of water molecules	29	
B factors		
Average of main chains	65.3	
Average of side chains	76.3	
Water molecules	65.4	
Geometric rmsd		
Bond length (Å)	0.007	
Bond angles (°)	1.2	

Fluorescence Microscopy

Cells were grown to midlog phase in selective media and viewed on an Olympus IX-70 fluorescence microscope (excitation, 560 nm; dichroic mirror at 595 nm; emission, 630 nm). Images were captured with an IMAGO charge-coupled device camera controlled by TILLvisION software (TILL Photonics, Eugene, OR) and were processed by using Adobe Photoshop 5.0 (Adobe Systems, Mountain View, CA).

CPY Maturation Assay

Yeast *vps27Δ hse1Δ* transformants were metabolically labeled with the ^{35}S Express reagent (Perkin Elmer Life Sciences) for 10 min (pulse) and chased for 30 min (Bonifacino and Dell'Angelica, 1998). Immunoprecipitations with mouse anti-CPY (Molecular Probes, Eugene, OR) were performed overnight at 4°C, and the immunoprecipitates were analyzed by SDS-PAGE and fluorography.

CPY Secretion Assay

The CPY secretion colony blot assay was performed as described (Mullins and Bonifacino, 2001). Strains were grown to 1–1.5 U of OD_{600}/ml at 30°C and were concentrated to 0.2 U of OD_{600}/ml. A total of 5 μl of each strain was spotted on selective medium. Plates were incubated overnight at 30°C to allow for cell growth, overlayed with nitrocellulose, and incubated 12–14 hr. Membranes were rinsed with distilled H_2O and were analyzed by immunoblotting with anti-CPY antibodies (Molecular Probes, Eugene, OR).

Simulations

To obtain a starting model, the Vps27 FYVE domain (Misra and Hurley, 1999) was docked to the membrane (Diraviyam et al., 2003). The Vps27 UIM1-ubiquitin complex and the Vps27 tandem UIM1-UIM2 constructs (Swanson et al., 2003) were used to model the ubiquitin complex with both Vps27 UIMs and the Hse1 UIM-ubiquitin complex. The Hse1 SH3 domain was modeled from the STAM2 SH3 domain (Kaneko et al., 2003). The VHS domains of Vps27 and Hse1 were modeled from the Hrs VHS domain (Mao et al., 2000). The core was positioned such that linkers to the nearest domains would be able to reach them. The predicted unstructured (Rost and Liu, 2003) C-terminal regions of Vps27/Hse1 were omitted.

Long-range electrostatic interactions were included at the Debye-Hückel level. The relative interaction strengths have previously been calibrated to reproduce measured protein second virial coefficients. Flexible linkers were represented as polymers at the amino acid level, and the folded protein domains were treated as rigid bodies. The resulting model has been validated by predictions of a series of protein-complex structures and binding affinities (Y.C.K. and G.H., unpublished data). Homology modeling was carried out manually in O (Jones et al., 1991) or semimanually in Coot (Emsley and Cowtan, 2004).

Protein-membrane interactions were represented by a combination of residue-dependent short-range interactions (Miyazawa and Jernigan, 1996) and a Gouy-Chapmann-type electrostatic potential between the flat membrane and the amino acids (Y.C.K. and G.H., unpublished data). To control molecular concentrations, the proteins were confined into semispheres of different sizes above the membrane plane. The FYVE domain was anchored to the membrane by a harmonic potential between the known PI(3)P-binding site (Misra and Hurley, 1999) and the membrane surface. The Ub-Cps1 molecules were modeled as a covalent link between Gly76 of ubiquitin and Lys8 of Cps1. Cps1 residues were modeled explicitly through residue 18, which was anchored to the membrane surface by a strict distance constraint.

An equilibrium ensemble of complex structures was obtained by performing replica-exchange Monte Carlo (MC) simulations, with 20 replicas covering the temperature range from 0.8*T*–1.7*T*, where *T* is room temperature. For each system, a total of 20,000–30,000 complex structures were obtained, which amounted to $\sim 10^7$–10^8 MC steps. To test for convergence, results from three independent runs were compared.

To gauge whether the simulations provided a realistic estimate of affinity, the affinities of the isolated UIMs for ubiquitin were calculated. We obtained a calculated value of $K_d = \sim 800$ μM for Vps27 UIM1, as compared to the experimental value of $K_d = \sim 300$ μM (Fisher et al., 2003). The calculated K_d of Vps27 UIM1 was lower than that of Vps27 UIM2, also in agreement with the experimental value (Fisher et al., 2003; Swanson et al., 2003). The simulations predicted the structure of the Vps27 UIM1-ubiquitin complex to within 3 Å rmsd (C_α) of the solution structure (Swanson et al., 2003). We found that the overall topology of the Vps27/Hse1 multiprotein complex inferred from known domain interactions was roughly maintained (Figure 7), despite substantial conformational dynamics. Ubiquitin-binding events were thoroughly equilibrated. These observations suggest that the simulations provide a well-sampled and quantitatively reasonable reflection of the system.

Supplemental Data

Supplemental Data include descriptions of methods and sedimentation equilibrium data and are available at http://www.developmentalcell.com/cgi/content/full/12/6/973/DC1/.

ACKNOWLEDGMENTS

We thank X. (Snow) Ren and W. Smith for assistance with biochemical experiments; R. Piper for strains and plasmids; J. Chrzas, J. Gonczy, M. Graham, and the entire staff of SER-CAT beamline ID-22 for user

support; and Y. Ye and A. Hickman for comments on the manuscript. Use of the Advanced Photon Source was supported by the U.S. Department of Energy, Basic Energy Sciences, Office of Science, under Contract No.W-31-109-Eng-38. This research was supported by National Institutes of Health intramural support, National Institute of Diabetes and Digestive and Kidney Diseases (J.H.H. and G.H.), National Institute of Child Health and Human Development (J.S.B.), and Intramural AIDS Targeted Antiviral Program (J.H.H. and J.S.B.).

Received: December 12, 2006
Revised: February 20, 2007
Accepted: April 18, 2007
Published: June 4, 2007

REFERENCES

Akutsu, M., Kawasaki, M., Katoh, Y., Shiba, T., Yamaguchi, Y., Kato, R., Kato, K., Nakayama, K., and Wakatsuki, S. (2005). Structural basis for recognition of ubiquitinated cargo by Tom1-GAT domain. FEBS Lett. *579*, 5385–5391.

Altschul, S.F., Madden, T.L., Schaffer, A.A., Zhang, J.H., Zhang, Z., Miller, W., and Lipman, D.J. (1997). Gapped BLAST and PSI-BLAST: a new generation of protein database search programs. Nucleic Acids Res. *25*, 3389–3402.

Babst, M. (2005). A protein's final ESCRT. Traffic *6*, 2–9.

Bilodeau, P.S., Urbanowski, J.L., Winistorfer, S.C., and Piper, R.C. (2002). The Vps27p-Hse1p complex binds ubiquitin and mediates endosomal protein sorting. Nat. Cell Biol. *4*, 534–539.

Bilodeau, P.S., Winistorfer, S.C., Kearney, W.R., Robertson, A.D., and Piper, R.C. (2003). Vps27-Hse1 and ESCRT-I complexes cooperate to increase efficiency of sorting ubiquitinated proteins at the endosome. J. Cell Biol. *163*, 237–243.

Bonifacino, J.S. (2004). The GGA proteins: adaptors on the move. Nat. Rev. Mol. Cell Biol. *5*, 23–32.

Bonifacino, J.S., and Dell'Angelica, E.C. (1998). Protein labeling and immunoprecipitation. In Current Protocols in Cell Biology, J.S. Bonifacino, M. Dasso, J.B. Harford, J. Lippincott-Schwartz, and K.M. Yamada, eds. (New York: John Wiley and Sons, Inc.), pp. 7.2.1–7.2.14.

Bowers, K., and Stevens, T.H. (2005). Protein transport from the late Golgi to the vacuole in the yeast *Saccharomyces cerevisiae*. Biochim. Biophys. Acta *1744*, 438–454.

Bowers, K., Lottridge, J., Helliwell, S.B., Goldthwaite, L.M., Luzio, J.P., and Stevens, T.H. (2004). Protein-protein interactions of ESCRT complexes in the yeast *Saccharomyces cerevisiae*. Traffic *5*, 194–210.

Brunger, A.T., Adams, P.D., Clore, G.M., DeLano, W.L., Gros, P., Grosse-Kunstleve, R.W., Jiang, J.S., Kuszewski, J., Nilges, M., Pannu, N.S., et al. (1998). Crystallography & NMR system: a new software suite for macromolecular structure determination. Acta Crystallogr. D Biol. Crystallogr. *54*, 905–921.

CCP4 (Collaborative Computational Project, Number 4) (1994). The CCP4 suite: programs for protein crystallography. Acta Crystallogr. A *50*, 760–763.

Clague, M.J., and Urbe, S. (2001). The interface of receptor trafficking and signalling. J. Cell Sci. *114*, 3075–3081.

Collins, B.M., Watson, P.J., and Owen, D.J. (2003). The structure of the GGA1-GAT domain reveals the molecular basis for ARF binding and membrane association of GGAs. Dev. Cell *4*, 321–332.

Demirov, D.G., and Freed, E.O. (2004). Retrovirus budding. Virus Res. *106*, 87–102.

Diraviyam, K., Stahelin, R.V., Cho, W., and Murray, D. (2003). Computer modeling of the membrane interaction of FYVE domains. J. Mol. Biol. *328*, 721–736.

Emsley, P., and Cowtan, K. (2004). Coot: model-building tools for molecular graphics. Acta Crystallogr. D Biol. Crystallogr. *60*, 2126–2132.

Fisher, R.D., Wang, B., Alam, S.L., Higginson, D.S., Robinson, H., Sundquist, W.I., and Hill, C.P. (2003). Structure and ubiquitin binding of the ubiquitin-interacting motif. J. Biol. Chem. *278*, 28976–28984.

Furey, W., and Swaminathan, S. (1997). PHASES-95: a program package for processing and analyzing diffraction data from macromolecules. Methods Enzymol. *277*, 590–608.

Gruenberg, J., and Stenmark, H. (2004). The biogenesis of multivesicular endosomes. Nat. Rev. Mol. Cell Biol. *5*, 317–323.

Haglund, K., Di Fiore, P.P., and Dikic, I. (2003). Distinct monoubiquitin signals in receptor endocytosis. Trends Biochem. Sci. *28*, 598–603.

Harper, J.W., and Schulman, B.A. (2006). Structural complexity in ubiquitin recognition. Cell *124*, 1133–1136.

Hershko, A., Ciechanover, A., and Varshavsky, A. (2000). The ubiquitin system. Nat. Med. *6*, 1073–1081.

Hicke, L. (2001). Protein regulation by monoubiquitin. Nat. Rev. Mol. Cell Biol. *2*, 195–201.

Hicke, L., Schubert, H.L., and Hill, C.P. (2005). Ubiquitin-binding domains. Nat. Rev. Mol. Cell Biol. *6*, 610–621.

Hirano, S., Kawasaki, M., Ura, H., Kato, R., Raiborg, C., Stenmark, H., and Wakatsuki, S. (2006). Double-sided ubiquitin binding of Hrs-UIM in endosomal protein sorting. Nat. Struct. Mol. Biol. *13*, 272–277.

Hochstrasser, M. (2000). Evolution and function of ubiquitin-like protein-conjugation systems. Nat. Cell Biol. *2*, E153–E157.

Holm, L., and Sander, C. (1995). Dali: a network tool for protein-structure comparison. Trends Biochem. Sci. *20*, 478–480.

Hurley, J.H., and Emr, S.D. (2006). The ESCRT complexes: structure and mechanism of a membrane-trafficking network. Annu. Rev. Biophys. Biomol. Struct. *35*, 277–298.

Hurley, J.H., Lee, S., and Prag, G. (2006). Ubiquitin binding domains. Biochem. J. *399*, 361–372.

Jones, T.A., Zou, J.Y., Cowan, S.W., and Kjeldgaard, M. (1991). Improved methods for building protein models in electron-density maps and the location of errors in these models. Acta Crystallogr. A *47*, 110–119.

Kaneko, T., Kumasaka, T., Ganbe, T., Sato, T., Miyazawa, K., Kitamura, N., and Tanaka, N. (2003). Structural insight into modest binding of a non-PXXP ligand to the signal transducing adaptor molecule-2 Src homology 3 domain. J. Biol. Chem. *278*, 48162–48168.

Kato, M., Miyazawa, K., and Kitamura, N. (2000). A deubiquitinating enzyme UBPY interacts with the Src homology 3 domain of Hrs-binding protein via a novel binding motif PX(V/I)(D/N)RXXKP. J. Biol. Chem. *275*, 37481–37487.

Katoh, Y., Shiba, Y., Mitsuhashi, H., Yanagida, Y., Takatsu, H., and Nakayama, K. (2004). Tollip and Tom1 form a complex and recruit ubiquitin-conjugated proteins onto early endosomes. J. Biol. Chem. *279*, 24435–24443.

Katzmann, D.J., Babst, M., and Emr, S.D. (2001). Ubiquitin-dependent sorting into the multivesicular body pathway requires the function of a conserved endosomal protein sorting complex, ESCRT-I. Cell *106*, 145–155.

Katzmann, D.J., Odorizzi, G., and Emr, S.D. (2002). Receptor downregulation and multivesicular-body sorting. Nat. Rev. Mol. Cell Biol. *3*, 893–905.

Katzmann, D.J., Stefan, C.J., Babst, M., and Emr, S.D. (2003). Vps27 recruits ESCRT machinery to endosomes during MVB sorting. J. Cell Biol. *162*, 413–423.

Kawasaki, M., Shiba, T., Shiba, Y., Yamaguchi, Y., Matsugaki, N., Igarashi, N., Suzuki, M., Kato, R., Kato, K., Nakayama, K., and Wakatsuki, S. (2005). Molecular mechanism of ubiquitin recognition by GGA3 GAT domain. Genes Cells *10*, 639–654.

Komada, M., and Kitamura, N. (2005). The Hrs/STAM complex in the downregulation of receptor tyrosine kinases. J. Biochem. (Tokyo) *137*, 1–8.

Liu, Y., and Eisenberg, D. (2002). 3D domain swapping: as domains continue to swap. Protein Sci. *11*, 1285–1299.

Lloyd, T.E., Atkinson, R., Wu, M.N., Zhou, Y., Pennetta, G., and Bellen, H.J. (2002). Hrs regulates endosome membrane invagination and tyrosine kinase receptor signaling in *Drosophila*. Cell *108*, 261–269.

Lu, Q., Hope, L.W.Q., Brasch, M., Reinhard, C., and Cohen, S.N. (2003). TSG101 interaction with HRS mediates endosomal trafficking and receptor down-regulation. Proc. Natl. Acad. Sci. USA *100*, 7626–7631.

Mao, Y.X., Nickitenko, A., Duan, X.Q., Lloyd, T.E., Wu, M.N., Bellen, H., and Quiocho, F.A. (2000). Crystal structure of the VHS and FYVE tandem domains of Hrs, a protein involved in membrane trafficking and signal transduction. Cell *100*, 447–456.

Mattera, R., Puertollano, R., Smith, W.J., and Bonifacino, J.S. (2004). The trihelical bundle subdomain of the GGA proteins interacts with multiple partners through overlapping but distinct sites. J. Biol. Chem. *279*, 31409–31418.

McCullough, J., Row, P.E., Lorenzo, O., Doherty, M., Beynon, R., Clague, M.J., and Urbe, S. (2006). Activation of the endosome-associated ubiquitin isopeptidase AMSH by STAM, a component of the multivesicular body-sorting machinery. Curr. Biol. *16*, 160–165.

Misra, S., and Hurley, J.H. (1999). Crystal structure of a phosphatidylinositol 3-phosphate-specific membrane-targeting motif, the FYVE domain of Vps27p. Cell *97*, 657–666.

Miyazawa, K., and Jernigan, R.L. (1996). Residue-residue potentials with a favorable pair term and an unfavorable high packing density term, for simulation and threading. J. Mol. Biol. *256*, 623–644.

Mizuno, E., Kawahata, K., Okamoto, A., Kitamura, N., and Komada, M. (2004). Association with Hrs is required for the early endosomal localization, stability, and function of STAM. J. Biochem. (Tokyo) *135*, 385–396.

Morita, E., and Sundquist, W.I. (2004). Retrovirus budding. Annu. Rev. Cell Dev. Biol. *20*, 395–425.

Mullins, C., and Bonifacino, J.S. (2001). Structural requirements for function of Yeast GGAs in vacuolar protein sorting, α-factor maturation, and interactions with clathrin. Mol. Cell. Biol. *21*, 7981–7994.

Pickart, C.M. (2001). Mechanisms underlying ubiquitination. Annu. Rev. Biochem. *70*, 503–533.

Piper, R.C., and Luzio, J.P. (2001). Late endosomes: sorting and partitioning in multivesicular bodies. Traffic *2*, 612–621.

Piper, R.C., Cooper, A.A., Yang, H., and Stevens, T.H. (1995). Vps27 controls vacuolar and endocytic traffic through a prevacuolar compartment in *Saccharomyces cerevisiae*. J. Cell Biol. *131*, 603–617.

Prag, G., Lee, S.H., Mattera, R., Arighi, C.N., Beach, B.M., Bonifacino, J.S., and Hurley, J.H. (2005). Structural mechanism for ubiquitinated-cargo recognition by the Golgi-localized, γ-ear-containing, ADP-ribosylation-factor-binding proteins. Proc. Natl. Acad. Sci. USA *102*, 2334–2339.

Puertollano, R. (2005). Interactions of Tom1L1 with the multivesicular body sorting machinery. J. Biol. Chem. *280*, 9258–9264.

Puertollano, R., and Bonifacino, J.S. (2004). Interactions of GGA3 with the ubiquitin sorting machinery. Nat. Cell Biol. *6*, 244–251.

Pullan, L., Mullapudi, S., Huang, Z., Baldwin, P.R., Chin, C., Sun, W., Tsujimoto, S., Kolodziej, S.J., Stoops, J.K., Lee, J.C., et al. (2006). The endosome-associated protein Hrs is hexameric and controls cargo sorting as a "master molecule". Structure *14*, 661–671.

Raiborg, C., Bremnes, B., Mehlum, A., Gillooly, D.J., D'Arrigo, A., Stang, E., and Stenmark, H. (2001). FYVE and coiled-coil domains determine the specific localisation of Hrs to early endosomes. J. Cell Sci. *114*, 2255–2263.

Raiborg, C., Bache, K.G., Gillooly, D.J., Madshus, I.H., Stang, E., and Stenmark, H. (2002). Hrs sorts ubiquitinated proteins into clathrin-coated microdomains of early endosomes. Nat. Cell Biol. *4*, 394–398.

Raiborg, C., Rusten, T.E., and Stenmark, H. (2003). Protein sorting into multivesicular endosomes. Curr. Opin. Cell Biol. *15*, 446–455.

Raiborg, C., Wesche, J., Malerod, L., and Stenmark, H. (2006). Flat clathrin coats on endosomes mediate degradative protein sorting by scaffolding Hrs in dynamic microdomains. J. Cell Sci. *119*, 2414–2424.

Ren, J., Kee, Y., Huibergtse, J.M., and Piper, R.C. (2007). Hse1, a component of the yeast Hrs-STAM ubiquitin sorting complex, associates with ubiquitin peptidases and a ligase to control sorting efficiency into multivesicular bodies. Mol. Biol. Cell *18*, 324–335.

Rost, B., and Liu, J.F. (2003). The PredictProtein server. Nucleic Acids Res. *31*, 3300–3304.

Schuck, P. (2003). On the analysis of protein self-association by sedimentation velocity analytical ultracentrifugation. Anal. Biochem. *320*, 104–124.

Scott, P.M., Bilodeau, P.S., Zhdankina, O., Winistorfer, S.C., Hauglund, M.J., Allaman, M.M., Kearney, W.R., Robertson, A.D., Boman, A.L., and Piper, R.C. (2004). GGA proteins bind ubiquitin to facilitate sorting at the trans-Golgi network. Nat. Cell Biol. *6*, 252–259.

Shiba, T., Kawasaki, M., Takatsu, H., Nogi, T., Matsugaki, N., Igarashi, N., Suzuki, M., Kato, R., Nakayama, K., and Wakatsuki, S. (2003). Molecular mechanism of membrane recruitment of GGA by ARF in lysosomal protein transport. Nat. Struct. Biol. *10*, 386–393.

Shiba, Y., Katoh, Y., Shiba, T., Yoshino, K., Takatsu, H., Kobayashi, H., Shin, H.W., Wakatsuki, S., and Nakayama, K. (2004). GAT (GGA and Tom1) domain responsible for ubiquitin binding and ubiquitination. J. Biol. Chem. *279*, 7105–7111.

Shih, S.C., Katzmann, D.J., Schnell, J.D., Sutanto, M., Emr, S.D., and Hicke, L. (2002). Epsins and Vps27p/Hrs contain ubiquitin-binding domains that function in receptor endocytosis. Nat. Cell Biol. *4*, 389–393.

Slagsvold, T., Pattni, K., Malerod, L., and Stenmark, H. (2006). Endosomal and non-endosomal functions of ESCRT proteins. Trends Cell Biol. *16*, 317–326.

Stahelin, R.V., Long, F., Diraviyam, K., Bruzik, K.S., Murray, D., and Cho, W. (2002). Phosphatidylinositol 3-phosphate induces the membrane penetration of the FYVE domains of Vps27p and Hrs. J. Biol. Chem. *277*, 26379–26388.

Suer, S., Misra, S., Saidi, L.F., and Hurley, J.H. (2003). Structure of the GAT domain of human GGA1: a syntaxin amino-terminal domain fold in an endosomal trafficking adaptor. Proc. Natl. Acad. Sci. USA *100*, 4451–4456.

Swanson, K.A., Kang, R.S., Stamenova, S.D., Hicke, L., and Radhakrishnan, I. (2003). Solution structure of Vps27 UIM-ubiquitin complex important for endosomal sorting and receptor downregulation. EMBO J. *22*, 4597–4606.

Tan, S. (2001). A modular polycistronic expression system for overexpressing protein complexes in *Escherichia coli*. Protein Expr. Purif. *21*, 224–234.

Terwilliger, T.C. (2000). Maximum-likelihood density modification. Acta Crystallogr. D Biol. Crystallogr. *56*, 965–972.

Weeks, C.M., and Miller, R. (1999). The design and implementation of *SnB* v2.0. J. Appl. Crystallogr. *32*, 120–124.

Weissman, A.M. (2001). Themes and variations on ubiquitylation. Nat. Rev. Mol. Cell Biol. *2*, 169–178.

Yamakami, M., Yoshimori, T., and Yokosawa, H. (2003). Tom1, a VHS domain-containing protein, interacts with tollip, ubiquitin, and clathrin. J. Biol. Chem. *278*, 52865–52872.

Zhu, G.Y., Zhai, P., He, X.Y., Terzyan, S., Zhang, R.G., Joachimiak, A., Tang, J., and Zhang, X.J.C. (2003). Crystal structure of the human GGA1 GAT domain. Biochemistry *42*, 6392–6399.

Accession Numbers

Crystallographic coordinates have been deposited in the Protein Data Bank with accession code 2PJW.

Developmental Cell *12*

Supplemental Data

The Vps27/Hse1 Complex Is a GAT Domain-Based Scaffold for Ubiquitin-Dependent Sorting

Gali Prag, Hadiya Watson, Young C. Kim, Bridgette M. Beach, Rodolfo Ghirlando, Gerhard Hummer, Juan S. Bonifacino, and James H. Hurley

Supplemental Experimental Procedures

Yeast Strains and Plasmid Construction

Yeast Strains. *Saccharomyces cerevisiae* strains were grown in standard yeast extract–peptone–dextrose (YPD) or synthetic medium with dextrose supplemented with the appropriate amino acids as required for plasmid maintenance. The following yeast strains were generous gifts from Robert Piper: *hse1*Δ*::Kanr* (PLY2464), *vps27*Δ*::LEU2* (PLY2228), and *hse1*Δ*::Kanr vps27*Δ*::LEU2* (PLY2784). These strains are derived from SF8389D (*MAT*α *ura3-52 leu2-3-112 his4-519 gal pep4-3*) and carry the *pep4* mutation to inactivate vacuolar proteases. For the pulse-chase CPY maturation assay, where functional proteases were needed, an *hse1*Δ*::Kanr vps27*Δ*::LEU2* strain was generated by PCR-mediated gene replacement of the *VPS27* locus in an *hse1*Δ*::Kanr* Research Genetics strain (MATα *his3*Δ*1 leu2*Δ*0 lys2*Δ*0 ura3*Δ*0*).

Yeast Plasmids. Hse1-myc (p1772) was a gift from Robert Piper. This plasmid is URA3-based (Bilodeau et al., 2002). *VPS27* was PCR-amplified from genomic DNA, using oligonucleotides that generated an EcoRI site at the 5' end, and an HA tag, followed by a stop codon and BamHI at the 3' end. The resulting PCR fragments were cloned into the EcoRI/BamHI sites of a pRS316 vector containing an ADH1 promoter (KpnI/EcoRI) and CYC1 terminator (XhoI/SacI) to generate Vps27-WT. QuikChange Mutagenesis (Stratagene) was used to generate the A266Q, L410D, I417D, and I420D mutations within Vps27-WT. For co-expression studies, KpnI/Sac II fragments from the Vps27-WT and mutant constructs were subcloned from pRS316 (ADH1/CYC1) into the KpnI/SacII sites within pRS413 vector. *STE3* and *CPS1* were PCR amplified from genomic DNA. *STE3* was cloned into the BamHI/XbaI sites of a pRS316 (ADH1/CYC1) vector containing a GFP fragment (XbaI/XhoI), generating Ste3p-GFP. *CPS1* was cloned into the BamHI/XhoI sites of a pRS316 (ADH1/CYC1) vector containing a GFP fragment (EcoRI/BamHI), generating GFP-Cps1p.

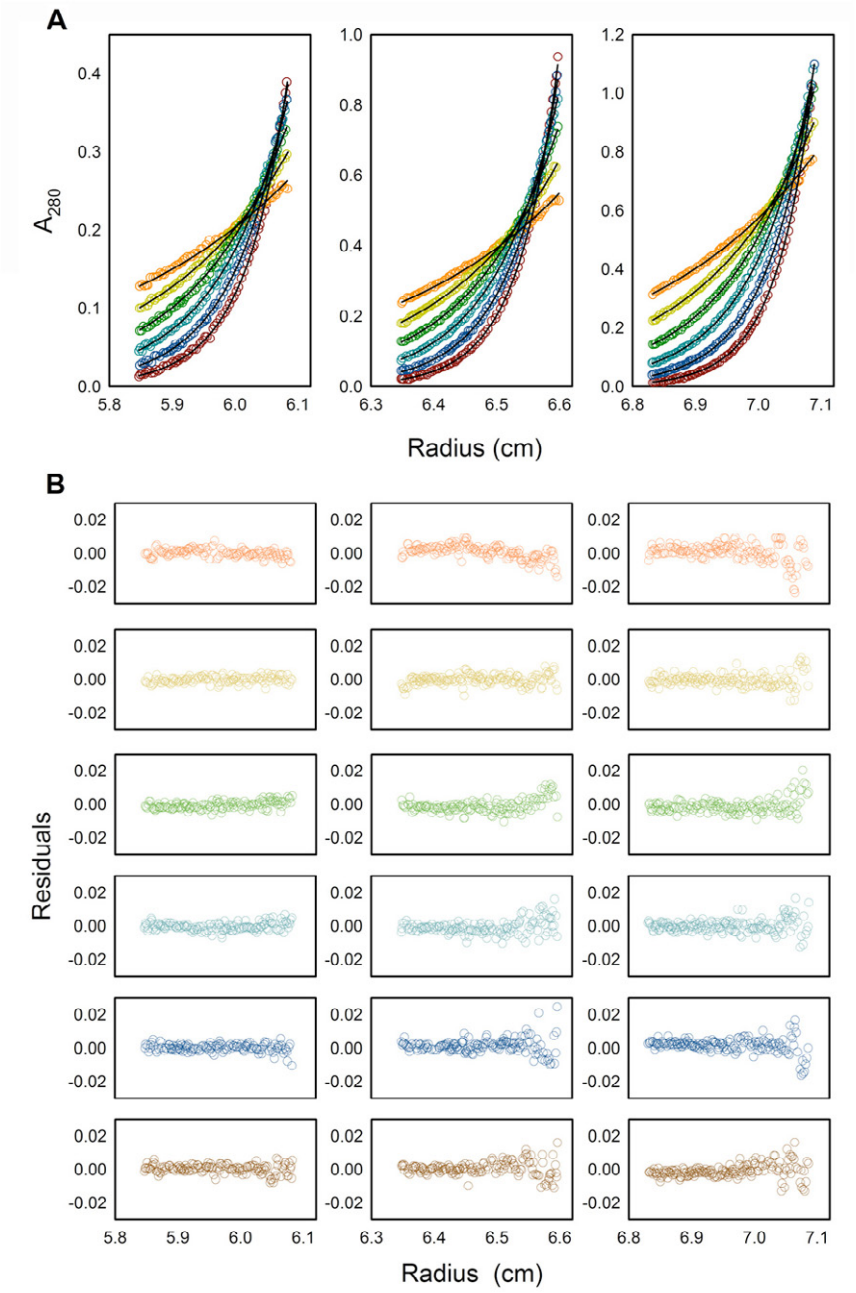

Figure S1. Vps27 and Hse1 Form a 1:1 Complex

(A) Sedimentation equilibrium profiles obtained for the Vps27 and Hse1 complex shown in terms of A_{280} versus the radius r for data collected at a loading A_{280} of 0.25 (left), 0.50 (center) and 0.75 (right). Data were collected at 4.0°C and rotor speeds of 13 (orange), 16 (yellow), 19 (green), 22 (cyan), 25 (blue) and 28 (brown) krpm and analyzed globally in terms of a single ideal solute. Best fits, corresponding to a molecular mass of 23.2 ± 0.4 kDa, are shown as black lines through the experimental points. For clarity, alternate data points have been omitted. The corresponding distributions of the residuals are shown in the accompanying plot (B).

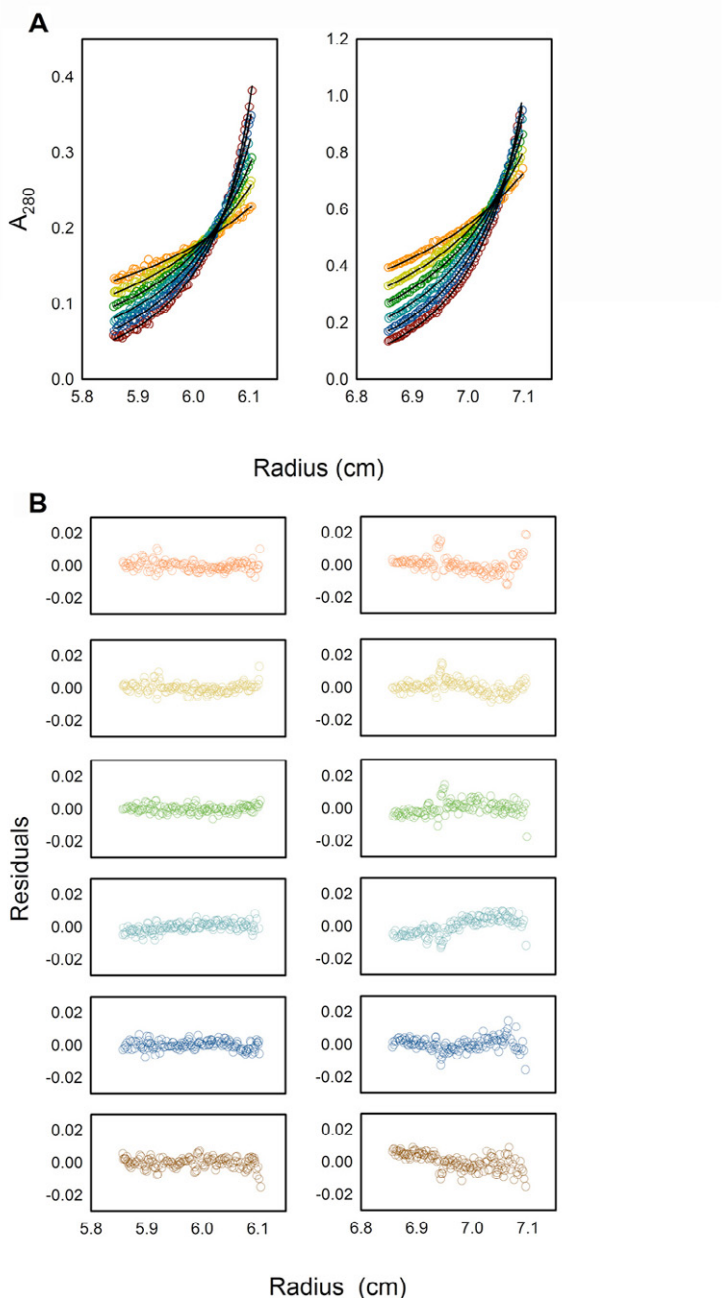

Figure S2. Isolated Vps27 Is Predominantly Monomeric

(A) Sedimentation equilibrium profiles obtained for the Vps27 shown in terms of A_{280} versus the radius r for data collected at a loading A_{280} of 0.20 (left) and 0.60 (right). Data were collected at 4.0°C and rotor speeds of 13 (orange), 16 (yellow), 19 (green), 22 (cyan), 25 (blue) and 28 (brown) krpm and analyzed globally in terms of two non-interacting ideal solutes using mass conservation. Best fits, corresponding to a Vps27 monomer and aggregate (n = 4.3, representing 20% of the total absorbance), are shown as black lines through the experimental points. For clarity, alternate data points have been omitted. The corresponding distributions of the residuals are shown in the accompanying plot (B).

Supplemental Reference

Bilodeau, P. S., Urbanowski, J. L., Winistorfer, S. C., and Piper, R. C. (2002). The Vps27p-Hse1p complex binds ubiquitin and mediates endosomal protein sorting. Nat. Cell Biol. *4*, 534-539.